ChemPubSoc Europe

DOI: 10.1002/open.201700106

Open Access ChemistryOPEN Full Papers

Two New Fluorogenic Aptasensors Based on Capped Mesoporous Silica Nanoparticles to Detect Ochratoxin A

Àngela Ribes,[a, b, c] Sara Santiago-Felipe,[a, b, c] Andrea Bernardos,[a, b, d] M. Dolores Marcos,[a, b, c, d] Teresa Pardo,[a, b, c, d] Félix Sancenón,[a, b, c, d] Ramón Martínez-Máñez,*[a, b, c, d] and Elena Aznar[a, b, c, d]

Aptamers have been used as recognition elements for several molecules due to their great affinity and selectivity. Additionally, mesoporous nanomaterials have demonstrated great potential in sensing applications. Based on these concepts, we report herein the use of two aptamer-capped mesoporous silica materials for the selective detection of ochratoxin A (OTA). A specific aptamer for OTA was used to block the pores of rhodamine B-loaded mesoporous silica nanoparticles. Two solids were prepared in which the aptamer capped the porous scaffolds by using a covalent or electrostatic approach. Whereas the prepared materials remained capped in water, dye delivery was selectively observed in the presence of OTA. The protocol showed excellent analytical performance in terms of sensitivity (limit of detection: 0.5–0.05 nM), reproducibility, and selectivity. Moreover, the aptasensors were tested for OTA detection in commercial foodstuff matrices, which demonstrated their potential applicability in real samples.

1. Introduction

Mycotoxins are metabolites produced by fungi species that are capable of causing disease and death in both humans and animals. They appear when food and feedstuff are stored or processed under environmental conditions that are favorable for fungi proliferation. The most common mycotoxins are ochratoxins, aflatoxins, fumonisins, trichothecenes, and zearalenone (Scheme 1).[1] Of these examples, ochratoxin A (OTA), produced by the *Aspergillus* and *Penicillium* strains, has been labeled as a carcinogen and nephrotoxic agent and is the most predominant contaminant in a wide variety of food commodities, such as cereals,[2,3] beverages, and dried fruits.[4] The European Commission's Scientific Committee on Food has established the maximum permitted content of OTA as 5 $\mu g\,kg^{-1}$ for raw cereal grains, 3 $\mu g\,kg^{-1}$ for all cereal-derived products, and 10 $\mu g\,kg^{-1}$ for soluble coffee.[5] A number of different techniques have been developed in recent years for the detection of OTA, most of which are based on gas chromatography/mass spectrometry (GC/MS)[6] and liquid chromatography (HPLC).[7,8] However, although these methods can correctly determine the presence of OTA, they require expensive equipment and complicated operator training.[9–11] In this scenario, the design of simple, yet selective and sensitive, probes for the detection of this carcinogenic agent is a field of interest.

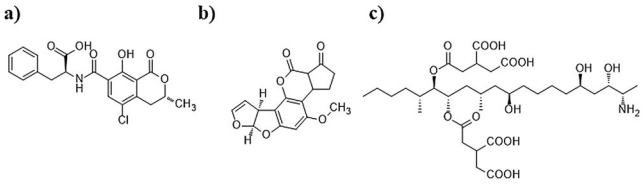

Scheme 1. Chemical structures of the most common micotoxins: a) ochratoxin A, b) aflatoxin B1, c) fumonisin B.

From another point of view, nanomaterials for sensing applications have played a great role in recent years due to their ca-

[a] À. Ribes, Dr. S. Santiago-Felipe, Dr. A. Bernardos, Prof. M. D. Marcos, Dr. T. Pardo, Prof. F. Sancenón, Prof. R. Martínez-Máñez, Dr. E. Aznar
Instituto Interuniversitario de Investigación de Reconocimiento Molecular y Desarrollo Tecnológico
Universitat Politècnica de València, Universitat de València
Camino de Vera s/n, 46022 Valencia (Spain)
E-mail: rmaez@qim.upv.es

[b] À. Ribes, Dr. S. Santiago-Felipe, Dr. A. Bernardos, Prof. M. D. Marcos, Dr. T. Pardo, Prof. F. Sancenón, Prof. R. Martínez-Máñez, Dr. E. Aznar
CIBER de Bioingeniería
Biomateriales y Nanomedicina (CIBER-BBN)
50018 Zaragoza (Spain)

[c] À. Ribes, Dr. S. Santiago-Felipe, Prof. M. D. Marcos, Dr. T. Pardo, Prof. F. Sancenón, Prof. R. Martínez-Máñez, Dr. E. Aznar
Unidad Mixta de Investigación en Nanomedicina y Sensores
Universitat Politècnica de València
Instituto de Investigación Sanitaria La Fe, 46022 Valencia (Spain)

[d] Dr. A. Bernardos, Prof. M. D. Marcos, Dr. T. Pardo, Prof. F. Sancenón, Prof. R. Martínez-Máñez, Dr. E. Aznar
Unidad Mixta UPV-CIPF de Investigación en Mecanismos de Enfermedades y Nanomedicina
Universitat Politècnica de València
Centro de Investigación Príncipe Felipe, 46022 Valencia (Spain)

Supporting Information and the ORCID identification number(s) for the author(s) of this article can be found under https://doi.org/10.1002/open.201700106.

pacity to provide rapid, simple, and sensitive responses to target analytes.[12–15] Moreover, of the nanomaterials used in sensing protocols, mesoporous silica nanoparticles (MSNs) have been widely employed due to some of their remarkable properties, such as large load capacity and the possibility to modify their surface easily with several groups due to the presence of silanol groups (SiOH), which have excellent reactivity.[16–24] Moreover, MSNs can be functionalized with different (bio)molecules that can act as "molecular gates" to obtain hybrid gated organic–inorganic capped supports for the design of systems able to release an entrapped payload upon the application of specific stimuli.[25] These gated supports have been widely used in the design of drug delivery carriers and to a lesser extent in sensing protocols.[26–30]

Additionally, the development of sensing materials by using aptamers as potential systems able to detect trace amounts of target substances has also attracted the attention of the research community.[31–36] Aptamers are stable DNA sequences with high affinity and selectivity for target biomolecules, small neutral molecules, or ions, and their use in the design of several sensors and probes has resulted in the development of highly sensitive systems for different analytes.[37–40] Recently, some aptasensors to detect OTA have been described.[41] However, to the best of our knowledge, the use of aptamer-based gated materials with MSNs for the fluorogenic detection of OTA has not yet been reported.

Based on these ideas, we report herein the development of two new gated materials based on MSNs loaded with a fluorophore (rhodamine B) and capped with an aptamer that is selective for OTA. It was also our aim to study different modes in which the aptamer can be used as a cap and its effect on the performance of the aptasensors. The materials were fully characterized and used for the selective and sensitive detection of OTA in spiked wheat samples.

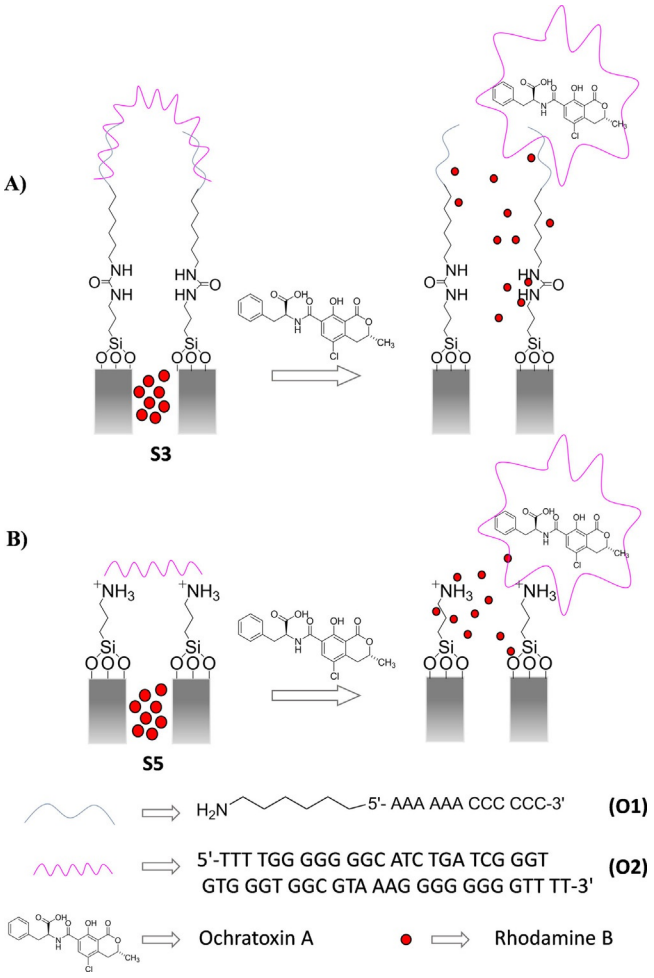

Scheme 2. Performance of gated materials A) **S3** capped with an aptamer in covalent approach and B) **S5** capped with an aptamer in electrostatic approach. Delivery of dye (rhodamine B) entrapped in **S3** and **S5** is selectively accomplished in the presence of OTA.

2. Results and Discussion

2.1. Preparation and Characterization of the Sensing Support

For the preparation of the sensing materials, two different approaches have been followed that involved two different methods to cap the pores with the OTA aptamer (Scheme 2). In both cases, MSNs of approximately 100 nm were selected as inorganic scaffolds and the pores were loaded with a fluorophore (rhodamine B).

In the first approach (referred to hereafter as the covalent approach; Scheme 2A), the external surface of the MSNs was functionalized with (3-isocyanatopropyl)triethoxysilane to give solid **S1**. In a subsequent step, a short DNA sequence, functionalized with an aminohexyl moiety at the 5′-end position (i.e. NH_2-$(CH_2)_6$-5′-AAA AAA CCC CCC-3′, **O1**) was covalently attached to **S1** through the formation of urea bonds to obtain solid **S2**. Then, a single-stranded oligonucleotide (i.e. 5′-TTT TGG GGG GGC ATC TGA TCG GGT GTG GGT GGC GTA AAG GGG GGG GTT TT-3′, **O2**), which contains the specific sequence of the OTA aptamer, was hybridized to the attached **O1** to obtain capped solid **S3**. In the second approach (referred to hereafter as the electrostatic approach; Scheme 2B), MSNs were functionalized with (3-aminopropyl)triethoxysilane to give solid **S4**. Aminopropyl moieties are partially charged at a neutral pH and are known to display electrostatic interactions with negatively charged aptamers. Based on this, addition of **O2** to suspensions of solid **S4** gave gated probe **S5**.

MSNs **S1**, **S2**, **S3**, **S4**, and **S5** were characterized by using standard techniques, such as powder X-ray diffraction (PXRD), transmission electron microscopy (TEM), N_2 adsorption–desorption isotherms, thermogravimetric analysis (TGA), dynamic light scattering (DLS), and Fourier transform infrared spectroscopy (FTIR).

The PXRD pattern of the as-synthesized MSNs (Figure 1, curve a) showed four low-angle reflections typical of a hexagonal array, indexed as (100), (110), (200), and (210) Bragg peaks. A significant displacement in the (100) peak in the PXRD pattern of the calcined MSNs was evident in Figure 1, curve b, and is related to a cell contraction (5 Å) due to the condensation of silanol groups during calcination. Figure 1, curves c–g, correspond to the XRD patterns of **S1**, **S2**, **S3**, **S4**, and **S5**. A de-

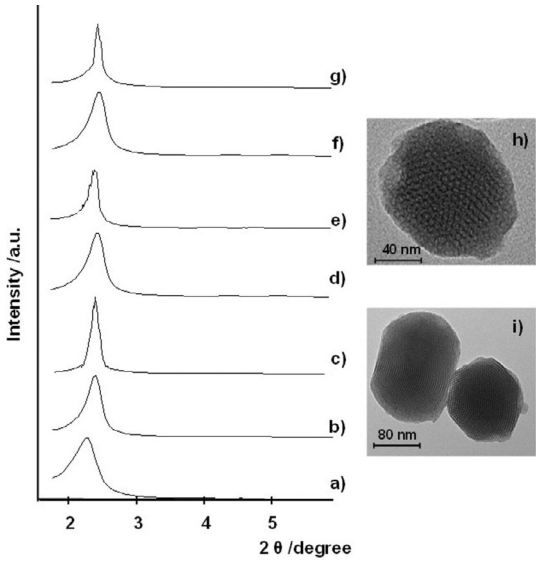

Figure 1. Powder X-ray diffraction patterns of a) as-formed MSNs, b) calcined MSNs, c) solid **S1**, d) solid **S2**, e) solid **S3**, f) solid **S4**, and g) solid **S5**. TEM images of h) calcined MSNs and i) **S3**.

crease in intensity of the (100) peak and a broadening of the (110) and (200) reflections was observed and are related to a loss of contrast due to filling the solid with the dye and capping the pores. Moreover, the presence of a mesoporous structure in calcined MSNs and final functionalized solids was confirmed by TEM analysis, in which the typical channels of a mesoporous silica matrix were clearly visualized (Figure 1h and i).

In addition, mesoporosity was analyzed by N_2 adsorption–desorption isotherms. For the starting calcined MSNs, a Brunauer–Emmett–Teller (BET) specific surface area of 908.6 $m^2 g^{-1}$ was obtained, whereas a decrease in the specific surface was observed for **S1** and **S4** and BET values of 112.7 and 414.7 $m^2 g^{-1}$ were found respectively (see Figure S1 and Table S1 in the Supporting Information). This is in agreement with the presence of the rhodamine B dye inside the pores and the surface functionalization. Moreover, the content of 3-isocyanatopropyl and 3-aminopropyl moieties, rhodamine B, **O1** and **O2** in the different prepared solids was calculated from thermogravimetric data (Table 1). By taking into account that the typical external surface of MSNs is 70 $m^2 g^{-1}$, an estimated capping density of 0.0029 $mmol_{O2} m^{-2}$ and 0.0014 $mmol_{O2} m^{-2}$ was calculated for solids **S3** and **S5**, respectively. The size of the nanoparticles was determined by using DLS studies. Diameters of 152, 162, 194, 379, 164, and 190 nm were found for starting calcined MSNs **S1**, **S2**, **S3**, **S4** and **S5**, respectively (see Figure S2 and Table S2 in the Supporting Information). Moreover, the presence of DNA in the prepared nanoparticles was confirmed by using FTIR spectroscopy (see Figure S3 and Table S3).

Table 1. Contents of 3-isocyanatopropyl, 3-aminopropyl, rhodamine B, **O1** and **O2** in the different prepared solids.

	Rhodamine B [mmol mg^{-1}]	3-Isocyanato-propyl [mmol mg^{-1}]	3-Amino-propyl [mmol mg^{-1}]	**O1** [mmol mg^{-1}]	**O2** [mmol mg^{-1}]
S1	0.024	0.024	–	–	–
S2	0.011	0.024	–	0.00009	–
S3	0.003	0.024	–	0.00009	0.0002
S4	0.003	–	0.020	–	–
S5	0.0008	–	0.020	–	0.0001

2.2. Release Experiments

Figure 2A shows the delivery kinetics profile of the dye from solid **S3** (covalent approach). In the absence of OTA (curve a), a poor rhodamine B release was observed, which indicated tight pore closure. However, payload delivery was clearly found when OTA was added to the solution (curve b).

Dye delivery was attributed to the displacement of aptamer **O2** induced when OTA was present in the solution due to aptamer–OTA binding (Scheme 2). A similar selective delivery in the presence of OTA was observed for solid **S5** (electrostatic approach). As depicted in Figure 2, dye delivery from solid **S3** reached 80% of the total amount of dye delivered after 10 min (Figure 2A), whereas a payload delivery of approximately 60% was observed from solid **S5** after the same time (Figure 2B).

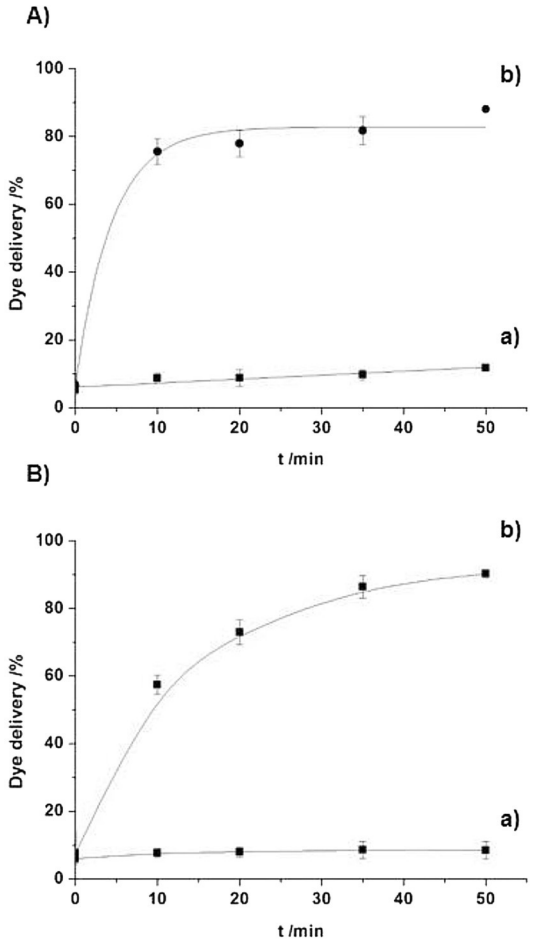

Figure 2. Release profile of rhodamine B from A) solid **S3** and B) solid **S5** in the absence (a) and presence (b) of OTA (5 μM) in hybridization buffer.

This difference in release rate should be ascribed to the different methods used to cap **S3** and **S5** (see below).

2.3. Sensitivity and Selectivity Studies

To assess the sensitivity of the method, the response of **S3** and **S5** to different concentrations of OTA was studied. It was found that the amount of rhodamine B delivered was proportional to OTA concentration, which is in agreement with the uncapping protocol detailed above. A limit of detection (LOD) of 0.5 nM was determined for **S3** (see Figure S4A), whereas for solid **S5**, a LOD as low as 0.05 nM was found (see Figure S4B). This difference in LOD is tentatively attributed to the weaker interaction of aptamer **O2** to the silica surface in the electrostatic approach (solid **S5**) compared with the covalent approach (solid **S3**). This weaker attachment of the aptamer to the surface favors the aptamer–OTA interaction, the displacement of the aptamer, and cargo delivery. However, both LOD values comply with those established by the legislation and are similar to or better than most published techniques for the detection of OTA (see Table S4).[42–54]

Additionally, the selectivity of **S3** (Figure 3 in black) and **S5** (Figure 3 in grey) to OTA was also studied. With this aim, cargo release from **S3** and **S5** was tested in presence of OTA, fumonisin B1 and aflatoxin B1. As shown in Figure 3, OTA was the only mycotoxin able to induce a notable dye delivery, whereas fumonisin B1 and aflatoxin induced negligible pore opening and poor payload release. This observation corroborates the selective OTA–aptamer interaction as the mechanism of the observed optical response.

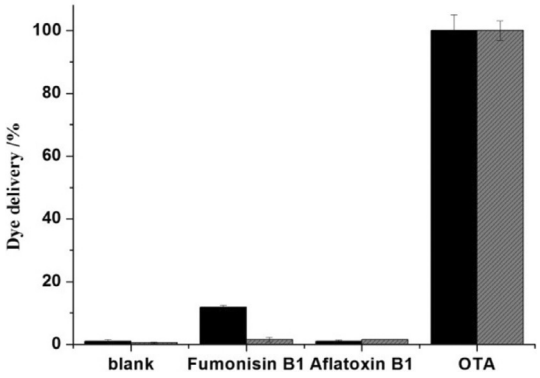

Figure 3. Release of rhodamine B from solid **S3** (in black) and **S5** (in grey) in the presence of OTA, aflatoxin B1, and fumonisin B1.

2.4. OTA Detection in Realistic Samples

Encouraged by these results, the potential use of **S3** to detect OTA in more competitive realistic samples was studied.[55] With this aim, the detection of OTA in wheat samples was evaluated by using an addition standard method. After OTA extraction, aliquots (100 μL) were spiked with different known amounts of a standard OTA solution (0, 10, 15, 20, 30, 50, 75 nM). In a following step, solid **S3** (100 μg) was added to each fraction and the volume was made up to a final value of 1000 μL with hybridization buffer. After 30 min at 25 °C, the release of rhodamine B from solid **S3** in the different aliquots was measured and a curve that followed the linear equation $y = 81.791x + 24870$ was obtained (see Figure S5A). From the intercept of the curve with the x axis, a concentration of OTA in the spiked sample of 372 nM was determined (93.05 % recovery). A similar procedure was followed by using solid **S5**. In this case, a recovery of 96.28 % was calculated (see Figure S5B). Use of the proposed aptasensor for the quantitative determination of OTA may provide a simple approach for food safety applications through the use of this simple, rapid, and sensitive assay. Moreover, as a preliminary study towards possible simple in situ applications, we have confirmed that **S3** and **S5** materials can be stored for weeks and then used without any changes in their sensing features.

3. Conclusions

We have developed two new fluorogenic aptasensors for the detection of OTA by using MSNs loaded with a dye and capped with an OTA-selective aptamer. Two approaches, based on an electrostatic or covalent protocol, were used to cap the pores. The response of both probes is related to the interaction between the capping aptamer and OTA, which induces displacement of the aptamer from the solid, opens the pores, and releases the dye. Although solid **S3** displayed dye delivery in a shorter time than **S5**, a lower LOD was observed for the latter. Specifically, a LOD as low as 0.5 nM for **S3** and 0.05 for **S5** were calculated. In addition, the capped nanomaterial allowed an accurate determination of OTA in realistic wheat samples. To the best of our knowledge, this is the first time that aptamer-capped mesoporous supports have been developed for the detection of OTA mycotoxin. Moreover, the method is simple, portable, can be easily tuned through the use of different reporting molecules (e.g., dyes, fluorophores, or electroactive species) and may allow the development of a simple test for the detection of OTA in food samples.

Experimental Section

General Techniques

PXRD, TEM, N_2 adsorption–desorption, TGA, DLS, FTIR, and fluorescence spectroscopy were employed to characterize the synthesized materials. PXRD measurements were performed by using a D8 Advance diffractometer with $Cu_{K\alpha}$ radiation (Philips, Amsterdam, The Netherlands). TGA was carried out by using a TGA/SDTA 851e balance (Mettler Toledo, Columbus, OH, USA) under an oxidizing atmosphere (air, 80 mL min^{-1}) with a heating gradient from 393–1273 K at 10 °C min^{-1}, followed by an isothermal heating step at 1273 °C for 30 min. TEM images were obtained by using a 100 kV CM10 microscope (Philips). N_2 adsorption–desorption isotherms were recorded by using an ASAP2010 automated adsorption analyzer (Micromeritics, Norcross, GA, USA). The samples were degassed at 120 °C under vacuum overnight. The specific surface areas were calculated from the adsorption data in the low pressure range by using the BET model.[56] Pore size was determined by using the Barret–Joyner–Halenda (BJH) method.[57] DLS was used to obtain the particle size distribution of the different solids by

using a Zetasizer Nano (Malvern Instruments, Malvern, UK). For the measurements, samples were dispersed in distilled water. Data analysis was based on the Mie theory by using refractive indexes of 1.33 and 1.45 for the dispersant and mesoporous silica nanoparticles, respectively. An adsorption value of 0.001 was used for all samples. Variation in this adsorption value did not significantly alter the obtained distributions. Measurements were performed in triplicate. FTIR spectra were acquired by using a Bruker Tensor II Platinum ATR spectrometer. Fluorescence spectroscopy measurements were carried out by using a Felix 32 Analysis version 1.2 (Build 56, Photon Technology International, Birmingham, NJ, USA).

Chemicals

Tetraethylorthosilicate (TEOS), *n*-cetyltrimethylammonium bromide (CTABr), sodium hydroxide (NaOH), triethylamine (TEA), (3-isocyanatopropyl)triethoxysilane, (3-aminopropyl)triethoxysilane, rhodamine B, tris(hydroxymethyl)aminomethane (TRIS), hydrochloric acid, ochratoxin A, fumonisin B1, and aflatoxin B1 were purchased from Sigma–Aldrich Química (Madrid, Spain). Oligonucleotides **O1** (NH_2-$(CH_2)_6$-5′-AAA AAA CCC CCC-3′) and **O2** (5′- TTT TGG GGG GGC ATC TGA TCG GGT GTG GGT GGC GTA AAG GGG GGG GTT TT-3′) were purchased from Isogen-Lifesciences (Barcelona, Spain). All products were used as received.

Synthesis of Mesoporous Silica Nanoparticles (MSNs)

CTABr (1.00 g, 2.74 mmol) was first dissolved in deionized water (480 mL). Then, NaOH (2.00 M, 3.5 mL) in deionized water was added, then the solution temperature was adjusted to 80 °C. TEOS (5 mL, 25.7 mmol) was then added dropwise to the solution of CTABr. The mixture was stirred for 2 h to give a white precipitate. Finally the solid product was centrifuged, washed with deionized water, and dried at 60 °C (as-synthesized MSNs). To prepare the final starting material, the as-synthesized solid was calcined at 550 °C under an oxidant atmosphere for 5 h to remove the template phase (calcined MSNs).

Synthesis of S1

Calcined MSNs (200 mg) and rhodamine B (766.4 mg, 0.16 mmol) were suspended in CH_3CN (10 mL), and the suspension was stirred at RT for 24 h. Then (3-isocyanatopropyl)triethoxysilane (247.6 μL, 1.0 mmol) was added, and the final mixture was stirred at RT for 5.5 h. The resulting pink solid (**S1**) was isolated by filtration, washed with CH_3CN (5 mL), and dried at 38 °C for 18 h.

Synthesis of S2

Oligonucleotide **O1** (10 μM, 100 μL) were added to a suspension that contained solid **S1** (1 mg), CH_3CN with rhodamine B (1 mM, 700 μL), and TEA (2 μL). The mixture was stirred for 3 h. The resulting material was isolated by centrifugation, washed with hybridization buffer to eliminate residual dye and free oligonucleotide, and dried under vacuum.

Synthesis of S3

Solid **S2** (100 μg) was suspended in hybridization buffer (297.5 μL) and **O2** (100 μM, 2.5 μL) was added to the reaction, then the mixture was stirred 2 h at RT. The resulting material was isolated by centrifugation, washed with hybridization buffer and dried under vacuum.

Synthesis of S4

Calcined MSNs (200 mg) and rhodamine B (766.4 mg, 0.16 mmol) were suspended in CH_3CN (10 mL). The suspension was stirred at RT for 24 h, then excess (3-aminopropyl)triethoxysilane (292.5 μL, 1 mmol) was added and the final mixture was stirred at RT for 5.5 h. The resulting pink solid (**S4**) was isolated by filtration, washed with CH_3CN (5 mL), and dried at 38 °C for 18 h.

Synthesis of S5

Solid **S4** (500 μg) were suspended in hybridization buffer (495 μL) and **O2** (100 μM, 5 μL) was added to the reaction, then the mixture was stirred for 30 min at 37 °C. The resulting material was isolated by centrifugation, washed with hybridization buffer, and dried under vacuum.

Assay Protocol

The response of solids **S3** and **S5** was tested in the presence of OTA by measuring the emission of rhodamine B delivered from the capped materials.

Solid S3

The material (100 μg) was suspended with hybridization buffer (400 μL; 20 mM Tris-HCl, 37.5 $MgCl_2$, pH 7.5) and divided into two aliquots (200 μL each). Then, aqueous OTA (500 μM, 10 μL) was added to one of the aliquots, whereas water (10 μL) were added to the other. In both cases, the volume was made up to 1000 μL with hybridization buffer. Suspensions were maintained at 25 °C and at certain times fractions were taken and centrifuged to separate the solid.

Solid S5

The material (500 μg) was suspended in hybridization buffer (1000 μL) and then separated into two aliquots (500 μL). The following steps were the same as for solid **S3**, described above, but the suspensions were maintained at 37 °C. Cargo release from the solids was measured by the rhodamine B fluorescence in the supernatants at $\lambda = 585$ nm ($\lambda_{ex} = 555$ nm).

Calibration Curve

Solid S3

The material (1 mg) was suspended in hybridization buffer (1000 μL) and separated into 10 aliquots (100 μL each). Different amounts of OTA standard solution were added to each aliquot and the volume was made up to 1000 μL with hybridization buffer. All samples were stirred at 25 °C for 30 min, and then centrifuged for 2 min at 12000 rpm to separate the solid. Finally, the fluorescence of the released rhodamine B was measured in the supernatants at $\lambda = 575$ nm ($\lambda_{ex} = 555$ nm).

Solid S5

The material (500 μg) was suspended in hybridization buffer (1000 μL) and separated into 10 aliquots (100 μL each). Different amounts of OTA standard solution were added to each aliquot and the volume was made up to 1000 μL with hybridization buffer. All samples were stirred at 37 °C for 30 min and centrifuged for 2 min at 12000 rpm to remove the solid. Finally, the fluorescence of the released rhodamine B was measured in the supernatants at $\lambda =$ 575 nm ($\lambda_{ex} =$ 555 nm).

Selectivity Studies with S3 and S5

To carry out these experiments, **S3** (400 μg) was suspended in hybridization buffer (400 μL) and separated into four aliquots (100 μL each). The suspensions of **S3** were spiked with OTA, fumonisin B1, or aflatoxin B1 (final concentration: 100 nM). In all cases, the volume was made up to 1000 μL with hybridization buffer. All samples were stirred at 25 °C for 30 min and centrifuged for 2 min at 12000 rpm to separate the solid. The fluorescence of the released rhodamine B was then measured in the supernatants at $\lambda =$ 575 nm ($\lambda_{ex} =$ 555 nm). The same protocol was carried out for solid **S5**, however, in this case the samples were stirred at 37 °C.

OTA Detection in Realistic Samples

For these experiments, OTA solution (10000 nM, 1000 μL) was added to wheat (0.05 g). The mixture was homogenized by using a vortex, then MeOH/H_2O (5 mL, 6:4 v/v) was added and the mixture was stirred for 30 min. Then solid was separated by centrifugation and the liquid phase was completely evaporated. The expected mycotoxin concentration (400 nM) was then determined by the standard addition method[55] by using solids **S3** and **S5**.

Acknowledgements

We thank the Spanish Government (projects MAT2015-64139-C4-1-R and AGL2015-70235-C2-2-R (MINECO/FEDER)) and the Generalitat Valenciana (project PROMETEOII/2014/047) for support. A.R. thanks UPV for her predoctoral fellowship. S.S. thanks the Instituto de Salud Carlos III and the European Social Fund for the financial support "Sara Borrell" (CD16/000237). A.B. thanks the Spanish Government for financial support by the "Juan de la Cierva-Incorporación" (IJCI-2014–21534). The authors also thank the Electron Microscopy Service at UPV for support.

Conflict of Interest

The authors declare no conflict of interest.

Keywords: aptamers · mesoporous materials · nanostructures · ochratoxin A · sensors

[1] J. Chen, Z. Fang, J. Liu, L. Zeng, *Food Control* **2012**, *25*, 555 – 560.
[2] L. Kupski, E. Badiale-Furlong, *Food chem.* **2015**, *177*, 354 – 360.
[3] G. Deng, K. Xu, Y. Sun, Y. Chen, T. Zheng, J. Li, *Anal. Chem.* **2013**, *85*, 2833 – 2840.
[4] C. Wang, J. Qian, K. Wang, K. Wang, Q. Liu, X. Dong, C. Wang, X. Huang, *Biosens. Bioelectron.* **2015**, *68*, 783 – 790.
[5] Commission Regulation, [EC] No. 1881/2006, 19 December, **2006**, setting maximum levels for certain contaminants in foodstuffs: *Off. J. Eur. Communities: Legis.* **2006**, *364*, 5 – 24.
[6] T. Tanaka, A. Yoneda, S. Inoue, Y. Sugiura, Y. Ueno, *J. Chromatogr. A* **2000**, *882*, 23 – 28.
[7] R. Ghali, I. Belouaer, S. Hdiri, H. Ghorbel, K. Maaroufi, A. Hedilli, *J. Food Compos. Anal.* **2009**, *22*, 751 – 755.
[8] F. Al-Taher, J. Cappozzo, J. Zweigenbaum, H. J. Lee, L. Jackson, D. Ryu, *Food Control* **2017**, *72*, 27 – 35.
[9] C. N. Rossi, C. R. Takabayaski, M. A. Ono, G. H. Saito, E. N. Itano, O. Kawamura, E. Y. Hirooka, E. Y. S. Ono, *Food Chem.* **2012**, *132*, 2211 – 2216.
[10] A. Sun, Y. Z. Zhang, G. P. Sun, X. N. Wang, D. Tang, *Biosens. Bioelectron.* **2017**, *89*, 659 – 665.
[11] K. E. Sapsford, C. R. Taitt, S. Fertig, M. H. Moore, M. E. Lassman, C. M. Maragos, L. C. Shriver-Lake, *Biosens. Bioelectron.* **2006**, *21*, 2298 – 2305.
[12] R. Wang, L. Xu, Y. Li, *Biosens. Bioelectron.* **2015**, *67*, 400 – 407.
[13] I. Willner, B. Shlyahovsky, M. Zayats, B. Willner, *Chem. Soc. Rev.* **2008**, *37*, 1153 – 1165.
[14] F. Sancenón, Ll. Pascual, M. Oroval, E. Aznar, R. Martínez-Máñez, *ChemistryOpen* **2015**, *4*, 418 – 437.
[15] E. Aznar, M. Oroval, Ll. Pascual, J. R. Murguía, R. Martínez-Máñez, F. Sancenón, *Chem. Rev.* **2016**, *116*, 561 – 718.
[16] J. L. V. Escoto, I. I. Slowing, B. G. Trewyn, V. S. Y. Lin, *Small* **2010**, *6*, 1952 – 1967.
[17] F. Tang, L. Li, D. Chen, *Adv. Mater.* **2012**, *24*, 1504 – 1534.
[18] H. Song, R. M. Rioux, J. D. Hoefelmeyer, R. Komor, K. Niesz, M. Grass, P. Yang, G. A. Somorjai, *J. Am. Chem. Soc.* **2006**, *128*, 3027 – 3037.
[19] A. Dandapat, D. Jana, G. De, *ACS Appl. Mater. Interfaces* **2009**, *1*, 833 – 840.
[20] M. H. Lim, C. F. Blanford, A. Stein, *J. Am. Chem. Soc.* **1997**, *119*, 4090 – 4091.
[21] M. H. Lim, C. F. Blanford, A. Stein, *Chem. Mater.* **1998**, *10*, 467 – 470.
[22] S. L. Burkett, S. D. Sims, S. Mann, *Chem. Commun.* **1996**, 1367 – 1368.
[23] C. E. Fowler, S. L. Burkett, S. Mann, *Chem. Commun.* **1997**, 1769 – 1770.
[24] B. H. Wouters, T. Chen, M. Dewilde, P. J. Grobet, *Microporous Mesoporous Mater.* **2001**, *44*, 453 – 457.
[25] F. Zhang, J. Cheng, R. Zhou, J. Cao, J. Li, C. Burda, Q. Min, J. Zhu, *Angew. Chem. Int. Ed.* **2014**, *53*, 2371 – 2375; *Angew. Chem.* **2014**, *126*, 2403 – 2407.
[26] S. Alberti, G. J. A. A. Soler-Illia, O. Azzaroni, *Chem. Commun.* **2015**, *51*, 6050 – 6075.
[27] C. H. Lu, B. Willner, I. Willner, *ACS Nano* **2013**, *7*, 8320 – 8332.
[28] R. Villalonga, P. Díez, A. Sánchez, E. Aznar, R. Martínez-Máñez, J. M. Pingarrón, *Chem. Eur. J.* **2013**, *19*, 7889 – 7894.
[29] L. Pascual, I. Baroja, E. Aznar, F. Sancenón, M. D. Marcos, J. R. Murguía, P. Amorós, K. Rurack, R. Martínez-Máñez, *Chem. Commun.* **2015**, *51*, 1414 – 1416.
[30] A. Ribes, E. Xifré-Perez, E. Aznar, F. Sancenón, T. Pardo, L. F. Marsal, R. Martínez-Máñez, *Sci. Rep.* **2016**, *6*, 38649 – 38658.
[31] M. Oroval, C. Coll, A. Bernardos, M. D. Marcos, R. Martinez-Mañez, D. G. Shchukin, F. Sancenón, *ACS Appl. Mater. Interfaces* **2017**, *9*, 11332 – 11336.
[32] M. Oroval, E. Climent, C. Coll, R. Eritja, A. Aviñó, M. D. Marcos, F. Sancenón, R. Martínez-Máñez, P. Amorós, *Chem. Commun.* **2013**, *49*, 5480 – 5482.
[33] W. Wang, T. Yan, S. Cui, J. A. Wan, *Chem. Commun.* **2012**, *48*, 10228 – 10230.
[34] V. C. Özalp, A. Pinto, E. Nikulina, A. Chuvilin, T. Schäfer, *Part. Part. Syst. Charact.* **2014**, *31*, 161 – 167.
[35] M. McKeague, M. C. DeRosa, *J. Nucleic Acids* **2012**, 78 – 98.
[36] M. McKeague, E. M. McConnell, J. Cruz-Toledo, E. D. Bernard, A. Pach, E. Mastronardi, X. Zhang, M. Beking, T. Francis, A. Giamberardino, A. Cabecinha, A. Ruscito, R. Aranda-Rodriguez, M. Dumontier, M. C. DeRosa, *J. Mol. Evol.* **2015**, *81*, 150 – 161.
[37] A. D. Ellington, J. W. Szostak, *Nature* **1992**, *356*, 850 – 852.
[38] C. Tuerk, L. Gold, *Science* **1990**, *249*, 505 – 510.
[39] J. Xue, H. Wu, Z. Chu, Y. Mei, J. Ye, R. Liu, C. Zhang, L. Peng, W. Zheng, F. Chen, *Microchim. Acta* **2013**, *180*, 109 – 115.
[40] K. V. Ragavan, L. S. Selvakumar, *Chem. Commun.* **2013**, *49*, 5960 – 5962.
[41] Z. Mei, H. Chu, W. Chen, F. Xu, J. Liu, H. Xu, R. Zhang, L. Zheng, *Biosens. Bioelectron.* **2013**, *39*, 26 – 30.

[42] L. Lv, D. Li, R. Liu, C. Cui, Z. Guo, *Sens. Actuators B* **2017**, *246*, 647 – 652.
[43] S. Hu, W. Ouyang, L. Guo, Z. Lin, X. Jiang, B. Qiu, G. Chen, *Biosens. Bioelectron.* **2017**, *92*, 718 – 723.
[44] M. A. Andrade, F. M. Lanças, *J. Chromatogr. A* **2017**, *1493*, 41 – 48.
[45] S. Joshi, R. M. Annida, H. Zuilhof, T. A. van Beek, M. W. Nielen, *J. Agric. Food Chem.* **2016**, *64*, 8263 – 8271.
[46] M. Mahdi, B. Mansour, M. Afshin, *Microchim. Acta* **2016**, *183*, 3093 – 3099.
[47] V. Pagkali, P. S. Petrou, A. Salapatas, E. Makarona, J. Peters, W. Haasnoot, G. Jobs, A. Economou, K. Misiakos, I. Rapti, S. E. Kakabakos, *J. Hazard. Mater.* **2017**, *323*, 75 – 83.
[48] P. Novo, G. Moulas, D. M. F. Prazeres, V. Chu, J. P. Conde, *Sens. Actuators B* **2013**, *176*, 232 – 240.
[49] A. Karczmarczyk, K. Haupt, K. H. Feller, *Talanta* **2017**, *166*, 193 – 197.
[50] A. Karczmarczyk, C. Reiner-Rozman, S. Hageneder, M. Dubiak-Szepietowska, J. Dostálek, K. H. Feller, *Anal. Chim. Acta* **2016**, *937*, 143 – 150.
[51] C. Zhang, J. Tang, L. Huang, Y. Li, D. Tang, *Microchim. Acta* **2017**, *184*, 2445 – 2453.
[52] Y. Ji, Q. He, Y. Xu, Z. Tu, H. Yang, Y. Qiu, X. Wang, Y. Liu, *Anal. Methods* **2016**, *8*, 7824 – 7831.
[53] H. Jiang, X. Li, Y. Xiong, K. Pei, L. Nie, Y. Xiong, *Toxins* **2017**, *9*, 83 – 94.
[54] J. Xu, W. Li, R. Liu, Y. Yang, Q. Lin, J. Xu, P. Shen, Q. Zheng, Y. Zhang, Z. Han, J. Li, T. Zheng, *Sens. Actuators B* **2016**, *232*, 577 – 584.
[55] J. V. Ros-Lis, B. García, D. Jiménez, R. Martínez-Máñez, F. Sancenón, J. Soto, F. Gonzalvo, M. C. Valldecabres, *J. Am. Chem. Soc.* **2004**, *126*, 4064 – 4066.
[56] E. P. Barrett, L. G. Joyner, P. P. Halenda, *J. Am. Chem. Soc.* **1951**, *73*, 373 – 380.
[57] S. Brunauer, P. H. Emmett, E. Teller, *J. Am. Chem. Soc.* **1938**, *60*, 309 – 319.

Received: May 29, 2017
Version of record online August 2, 2017

